Load-bearing Capacity and Fracture Behaviour of Notched Cross Laminated Timber Plates

Alen Malagic [1)], Manfred Augustin [1)], Gregor Silly [1)], Alexandra Thiel [1)], Gerhard Schickhofer [1),2)]

[1)] holz.bau forschungs gmbh, Competence Centre of Timber Engineering and Wood Technology, Graz, Austria

[2)] Institute of Timber Engineering and Wood Technology, Faculty of Civil Engineering, Graz University of Technology, Graz, Austria

Keywords: cross laminated timber, notch, fracture mechanics, beam on elastic foundation, elastic interface, elastic clamping

1 Introduction

Abrupt changes in the geometry of load-bearing members (e.g., notches, holes), also referred as geometric discontinuities, induce high stress concentrations and high stress gradients in localised area of members. In a good engineering practice one should aim towards avoiding such discontinues in a first place. Nonetheless due to numerous constraints during planning and construction process this is not always possible. In buildings with Cross Laminated Timber (CLT) such examples occur e.g. in connections of slab-slab and wall-slab systems (Figure 1).

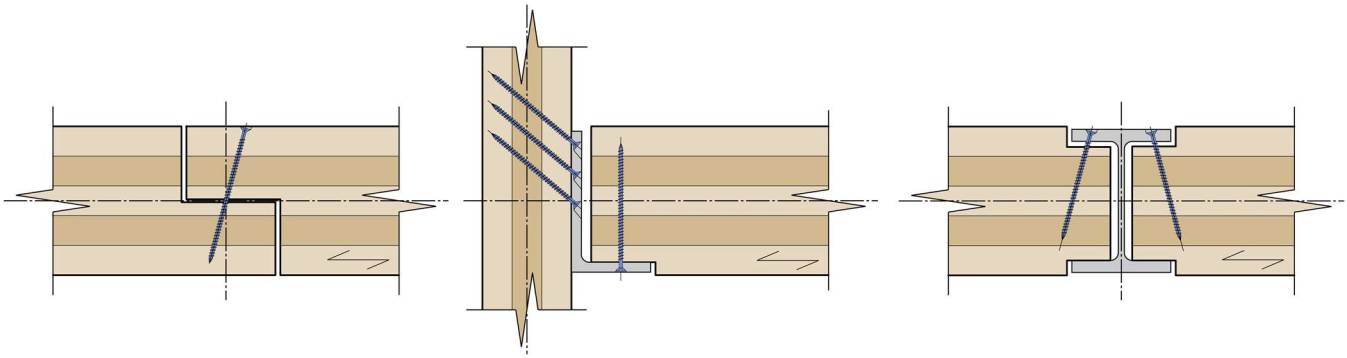

Figure 1 Various types of notches in CLT plates; a) Connection of two CLT plates. b) Connection of a CLT plate with a steel L-profile. c) Connection of CLT plates with a steel I-profile.

When loaded up to a certain level, a crack will be induced at the notch tip due to the combined local stress concentrations in tension perpendicular to grain and shear, latter, depending upon layer orientation result in longitudinal or rolling shear stresses. The crack propagation leads to unstable and fast delamination of the member and subsequently to its failure, if the residual strength of the member above the crack isn't sufficient. The failure of the notch is therefore viewed as brittle.

The aim of this work is to provide a new analytical approach for unreinforced CLT notches based on Beam on Elastic Foundation (BEF). The analytical approaches are verified with an extensive base of test results. Moreover, the aim is to verify the analytical model referred as Structural Element Model developed by Serrano (2019, 2020) with additional test results. At the end, conclusions and suggestions for the design and calculation of CLT notches are given.

2 State of the art

The models in this chapter and in section 4.2 are developed in a scope of linear elastic fracture mechanics (LEFM) and energy balance method. In this method the failure load at the crack tip is obtained according to the breakthrough work in fracture mechanics, i.e. work of Griffith (1921). The condition for crack growth of an initial crack at the notch according to LEFM is fulfilled, when the difference between the potential energy U_e and the strain energy U_i is equal to the energy dissipated by the crack during an infinitesimal increase in crack area $B \cdot da$. In scope of LEFM this energy is represented as energy release rate (ERR) G and defined as

$$G = \frac{1}{B}\left(\frac{dU_e}{da} - \frac{dU_i}{da}\right). \tag{1}$$

Failure occurs when the ERR is equal to the energy crack resistance, also known as fracture energy G_f, which is a material property obtained from experiments. In scope of LEFM it is assumed that $G_f = G_c$. Further, in this paper it is implied that the crack grows only due to the crack opening in Mode I, leading to $G_f = G_{c,I}$. With further development of Eq. (1) considering the substitution of $C = \delta/V$ the failure load according to LEFM is obtained as

$$V_f = \sqrt{\frac{2BG_c}{\frac{dC}{da}}}, \tag{2}$$

where C denotes the compliance of the structure, B the width of the member and V_f the failure load at the support, while the vertical displacement at the loading point is represented by δ.

Through the history the design equations for timber notches have improved from empirical to analytical approaches derived from fracture mechanics. Development culminated with the analytical solution from Gustafsson (1988), later implemented in Eurocode 5 (EC5) for notches in solid timber, laminated veneer lumber (LVL) and

glulam. The approach is based on the energy balance of the end notched beam at the crack tip derived from (LEFM) and the Timoshenko beam theory. The design expression in Eq. (3) represents the solution given in EC5 (Eurocode 5, 2004); for a detailed derivation of Eq. (3) refer to Serrano (2019).

$$\tau_d = \frac{1.5 V_f}{B\alpha h} \leq k_v f_{v,d}\,, \tag{3}$$

where k_v is the strength reduction factor given by

$$k_v = \min\left\{ \frac{1}{\dfrac{k_n\left(1+\dfrac{1.1 i^{1.5}}{\sqrt{h}}\right)}{\sqrt{h}\left(\sqrt{\alpha-\alpha^2}+0.8\beta\sqrt{\dfrac{1}{\alpha}-\alpha^2}\right)}} \right. , \quad \mathrm{k_n} = \begin{cases} 4.5 & \text{for LVL} \\ 5.0 & \text{for solid timber} \\ 6.5 & \text{for glulam} \end{cases} \tag{4}$$

where i is the slope of the taper and k_n being the material parameter depending upon fracture energy defined as

$$k_n = 1.5\frac{\sqrt{\dfrac{G_c G_0}{0.6}}}{f_v}\,. \tag{5}$$

The geometric parameters of the notch α, β and i are explained in Figure 2b.

2.1 Current design of notched CLT plates

Current design equations for notches in CLT are given in ETA-06/0138 (2017) and Wallner-Novak et al. (2013) based on Eq. (3), but modified with $f_{v,r,d}$ instead of $f_{v,d}$. Approaches for CLT differ one from other in different definition of the effective height h_{ef} as shown in Figure 2a, subsequently leading to different material factors k_n as follows:

$$\mathrm{k_n} = \begin{cases} 4.5 & \text{for Wallner - Novak} \quad (\mathrm{WN}) \\ 4.7 & \text{for ETA - 06 / 0138} \quad (\mathrm{ETA}) \end{cases}$$

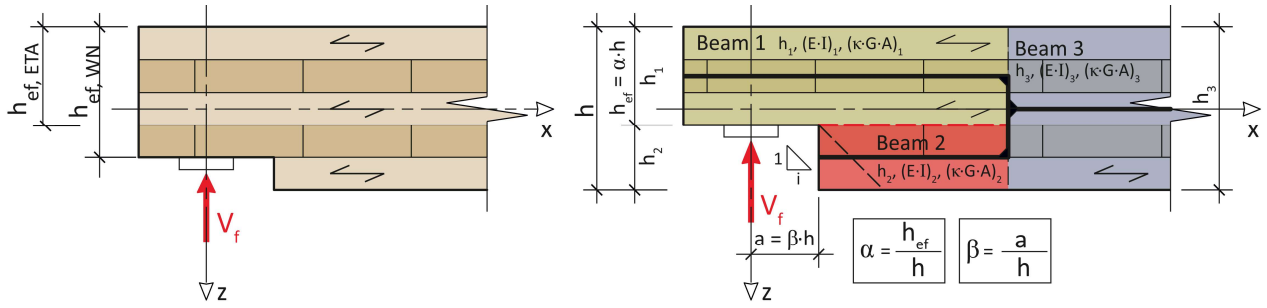

Figure 2 a) Different definitions of the effective notch height h_{ef}. b) Notch in a CLT plate

The major drawback of the mentioned approaches is the assumption that Gustafsson´s model can be modified by calibrating the material parameter k_n for CLT, following the example for k_n in EC5. However, such assumption in EC5 is only valid as calibrations are

made for beams which in general provide homogenous response in addition to constant ratios of material properties ($E_0/G_{0,90}$) and constant fracture properties of the material along the height of the member h_{ef}. For CLT the mentioned ratios and fracture properties derived as constant in Eq. (4) change with notch height h_{ef} depending on the position of longitudinal and transversal layers, the layup and number of layers in the member. These parameters of notched CLT elements result in a fundamentally different load-bearing capacity and fracture behaviour compared to e.g. notches in glulam. As reported in Serrano (2019) the approach for the fitting parameter k_n can only be applied on a limited number of layups. Consequently, a new and theoretically consistent approach is needed.

2.1.1 Structural Element Model

The Structural Element Model was developed by Serrano (2019) for this design situation and is represented by two Timoshenko beam elements connected with an elastic spring and a dummy rigid rod (see Figure 3). Calculating the energy release rate according to Eq. (2) and assuming that elastic spring k_φ approaches infinity, the failure load is obtained as

$$V_f = \sqrt{\frac{2BG_c}{\left(\frac{1}{(\kappa GA)_1}-\frac{1}{(\kappa GA)_3}\right)+(\beta h+\Delta a)^2\left(\frac{1}{(EI)_1}-\frac{1}{(EI)_3}\right)}}\,, \tag{6}$$

where $(\kappa GA)_1$, $(\kappa GA)_3$ are the shear stiffnesses and $(EI)_1$, $(EI)_3$ are the bending stiffnesses. Beam 1 represents the part of the member above the crack, while beam 3 is the full uncracked cross section of the CLT member in front of the crack.

The compliance C for this system takes into account the bending and shear part of the deformation calculated according to Timoshenko's theory.

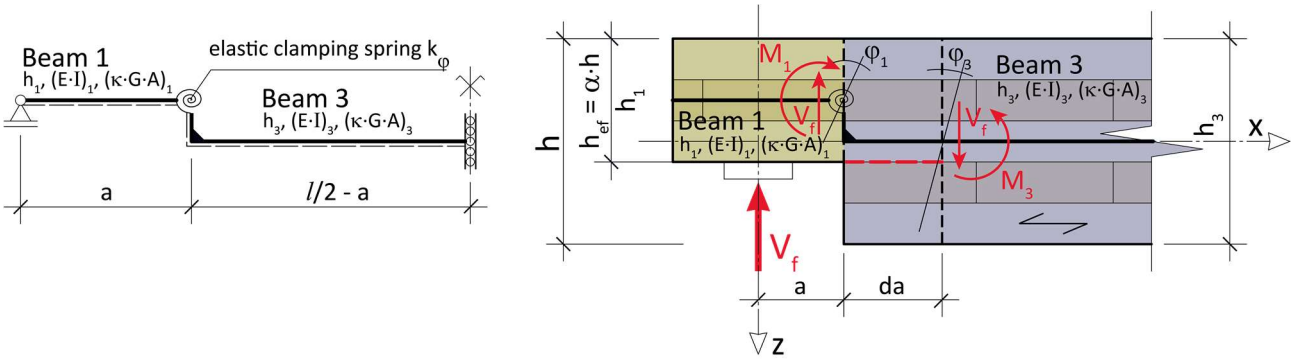

Figure 3 Structural Element Model developed by Serrano (2019, 2020)

The elastic spring k_φ simulates the additional rotation of the cross section at the crack tip due to the abrupt change in the cross section resulting in additional deformation and compliance. The elastic constant k_φ can be derived from numerical investigations as was done in Gustafsson (1988) for homogenous beams; for more details see Serrano (2019). An alternative approach would be to increase the crack length in order to

correctly represent the higher compliance. Modifying the crack length is appropriate for engineering practice as the closed form solution is simplified.

In the Structural Element Model the additional rotation is considered with increased fictitious crack length. Initial crack length βh is increased by the value $\Delta a = (1-\alpha)h$. The parameter Δa is determined as best fit to the test results from Friberg (2017), Serrano (2020) and numerical investigations based on LEFM. It is noted again that the fitting factor in Serrano (2019, 2020) is developed and verified only on a limited number of layups and notch parameters. Therefore further experimental investigations are presented in chapter 3 and compared with predictions of the model in section 5.1 with an objective to check the robustness of the current fitting parameter. In addition, an analytical model is presented taking into account the rotation at the crack tip in section 4.2.1 in order to verify the value of Δa.

3 Experimental program

3.1 General

The layered structure of CLT causes additional difficulties on keeping analytical approaches simple for engineering use and reliable in domain of significant parameters. In order to keep the design simple, it is inevitable to fit the necessary parameters by means of experimental results.

The currently available experimental results regarding notches in CLT are scarce. As known to the authors only Friberg (2017) and Serrano (2020) published results of tests on 5-layered CLT beams with different geometry parameters (α, β) (from which they derived the fitting parameter Δa in Eq. (6)). To overcome this lack of data and in order to get a more extensive view on the behaviour of CLT with notches an extensive test program, described in the next section, varying a broad range of key parameters was conducted.

3.2 Test program, methods and results

In total 192 CLT specimens without glued edge bonding, split up into 17 series with unreinforced notches and 7 series with reinforced notches were tested. To quantify the reduction of the load-bearing capacity of CLT plates with notches in comparison to plates without notches, the reference tests (in total 6 series referred in Table 1 with REF) were carried out. All the 33 specimens of these series failed in rolling shear. The reduction of the mean load-bearing capacity referenced to the mean rolling shear capacity of the reference series (without notches) will be denoted in Table 2 and Table 3 as $V_{f,\,mean} / V_{f,\,ref}$. An overview about the different series, their layup and their heights is given in Table 1.

Table 1. Overview of test series

	Series	Layup[a)]	h [mm]	B [mm]
3S	REF, 3A	40-40-40	120	600
5S	REF, 5A, 5B, 5C, 5D, 5E, 5F, 5A-R1, 5A-R2, 5A-R3, 5C-R1, 5C-R2	30-30-30-30-30	150	
	REF, 5G	30-30-30-30-30	150	
	REF, 5H, 5I, 5J, 5K, 5L	40-20-40-20-40	160	
7S	REF, 7A, 7B, 7A-R	30-30-30-30-30-30-30	210	
	REF, 7C, 7D, 7C-R	30-30-30-30-30-30-30	210	

a) underline refers to cross layer

All tests were done using a 4-point bending configuration (Figure 4) under controlled displacement. The specimens were notched on both ends in order to reduce material usage. The crack propagation was limited to the point of the first load introduction from the notch (3h), using self-tapping screws with the aim to preserve an intact cross section in the areas relevant for testing the notch on the opposite side of the specimen. The same test configuration depicted in Figure 4 was used for all series.

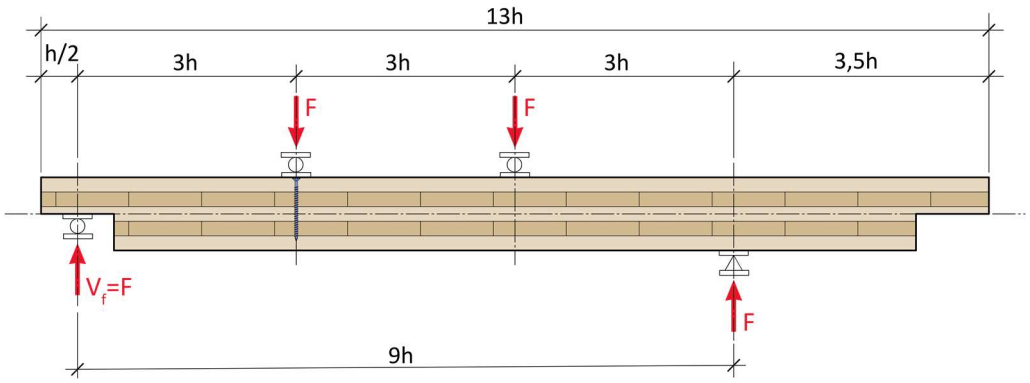

Figure 4 Test configuration for unreinforced and reinforced notches

In order to deduct a suitable test configuration, in a first step the influence of the specimen width B on the statistical parameters was investigated on 150 mm and 600 mm wide CLT members. From the statistical analysis it was found that the coefficient of variation was 18 % for the former and 7 % for the latter. Thus it was concluded that the width of 600 mm was optimal for the main testing program.

All tests were monitored by means of a digital image correlation system (DIC) with its help the correct crack lengths can be determined at the failure. In addition DIC was used to determine the strain distributions in vicinity of the notch. In particular the influence of growth ring pattern and stiffness in the radial and tangential direction of the cross layer could be tracked. This was important for the correct depiction of failure and crack propagation there. However, it should be mentioned that the influence of the free surface potentially can cause faulty representation of the real stress states and crack lengths thus limiting the reliability of measurements with the DIC.

3.3 Test results

3.3.1 Test results on unreinforced notches

In Table 2 the results of the test series with unreinforced notches are listed.

Table 2. Detailed results of tests on unreinforced notches

Series	Company	Num. of tests	β	α	$V_{f,mean}$ [kN]	CoV [%]	$V_{f,005}$ [kN]	MIN/MAX [kN]	$V_{f,mean}$ / $V_{f,ref}$ [%]
REF	1	6	-	-	67.0	6.39	58.7	63.0/75.3	100
3A		10	0.40	0.75	67.0	13.4	50.2	53.0/82.6	100
REF	2	6	-	-	107	3.13	99.8	101/111	100
5A		10	0.40	0.50	48.1	13.2	36.3	37.5/60.5	45.0
5B		10	0.20	0.60	73.9	7.77	63.1	61.5/83.5	69.0
5C		10	0.40	0.60	70.7	8.51	59.5	64.0/82.5	66.1
5D*		9	0.40	0.60	71.4	5.53	64.0	66.0/79.5	66.8
5E		6	0.40	0.80	76.7	8.14	64.6	67.5/84.5	71.7
5F		7	0.40	0.90	115	3.65	107	109/122	106
REF	2	5	-	-	74.5	4.46	68.0	69.5/79.0	100
5G		10	0.40	0.5	25.1	7.96	21.4	21.7/28.8	33.7
REF	3	4	-	-	133.0	1.73	128	130/135	100
5H		10	0.80	0.63	58.2	16.6	40.1	46.0/75.0	43.7
5I		8	0.40	0.63	58.0	8.71	48.4	51.3/66.1	43.4
5J		10	0.40	0.81	105	9.63	85.8	88.0/126	78.7
5K	4	6	0.40	0.63	83.5	7.00	72.5	72.7/90.9	62.8
5L		6	0.40	0.53	53.0	10.0	42.0	46.1/60.0	39.8
REF	5	6	-	-	113	8.47	94.2	95.5/125	100
7A		6	0.40	0.62	75.1	4.74	68.2	72.0/82.5	66.5
7B		6	0.40	0.71	95.8	5.07	86.4	87.0/103	84.8
REF	6	6	-	-	144	2.98	135	137/150	100
7C		6	0.40	0.57	72.9	7.59	61.1	63.0/79.5	64.5
7D		6	0.40	0.76	109	4.33	98.9	101/117	96.3

*Notch is tapered with i = 1.0, for definition of parameter *i* see Figure 2b)

3.3.1.1 Results

In series 5I, 5K the geometrically equivalent configurations showed high difference in the failure loads. The failure load in series 5K was 1.4 times higher than in 5I, possible cause is lower fracture energy of series 5I. This conclusion is derived from comparison of the test results with analytical and numerical results in section 5.1.

The influence of the notch length as well as the notch taper was investigated in series 5B, 5C, 5D*. As can be seen a notch tapered at 45° (i = 1.0) had only minor influence on the increase of load-bearing capacity compared to series 5C. It can be concluded from the tests, that tapering the notches with slopes i < 1.0 is not sufficient for an increase of the load-bearing capacity. Further tests on tapered specimens (i > 1.0) should be conducted and can be recommended in other to create a basis for the calibration of the load-bearing capacity compared to notches without taper.

Based on the formulation provided in EC5 for the influence of the notch taper on increase of load-bearing capacity ($1+1.1i^{1.5}/\sqrt{h}$) an increase of 9 % can be computed. Although the formulation overestimates the load-bearing capacity it seems to be a solid basis for further calibration based on experimental results of tapered CLT notches.

A similar diminishing return on the increase of the failure load could be recognised by varying the notch parameter β. For series 5B ($\beta = 0.2$), the failure load increased by 4 % compared to 5C ($\beta = 0.4$). For comparison the analytical approaches lead to around 5 % increase. A similar behaviour was recognised in series 5H and 5I, however it should be noted that the results in series 5I are probably influenced by the lower fracture energy.

3.3.1.2 Fracture behaviour of unreinforced notches

A consistent fracture behaviour of the specimens was observed through the experimental program. Two specific failure modes were observed as already reported in Serrano (2019, 2020):

- Fracture along the grain, if the notch was placed in a longitudinal layer or at the bottom of a longitudinal layer at the interface. The crack propagation can deviate due to the local grain angle deviations, however the propagation to adjacent transversal layer due to local grain deviations was not observed. Such behaviour occurred in cases when the notch was placed in the longitudinal layer but close to the interface (e.g. for series 7D). In some tests, due to the grain deviations, the crack kinked into the transversal layer. However, such behaviour took place after the crack propagated for several centimetres and during the unstable crack propagation, thus not influencing the load-bearing capacity.
- Fracture in the transversal layer, if the notch is placed in a transversal layer or at the bottom of a transversal layer at the interface. In general the crack propagation can be assumed at an angle of 45° to the horizontal. Nevertheless, in the transversal layer the crack propagation was heavily influenced by the grain pattern, and the location of the notch within the transversal layer. This behaviour can be explained by the heterogenous ratios of E_{90R}/E_{90T} and G_{90R}/G_{90T}. Several failure patterns were recognised from the tests regarding the crack propagation depending on the grain pattern at the notch tip in the transversal layer (Figure 5, middle). Different crack patterns were observed for series 5E, while for series 5G almost all failures occurred at an angle of 45° and some in a zig-zag manner as shown in Figure 5, middle.
- At some specimens a debonding of the glued interface was observed, pointing out that the fracture energy of the glued interface plays an important role in the area of the interface.

In series with notch in transversal layer 5E no significant increase of the load-bearing capacity was observed compared to its adjacent notch configuration in longitudinal layer 5C. This implies once more the negligible influence of transversal layers on the load-bearing capacity.

For the series 5F and 3A rolling shear before notch failures occurred. Implying that in CLT if only part of the first layer, e.g. 80 % is notched with $\beta < 0.5$, the rolling shear failure is the dominant mode of failure. This hypothesis should be nevertheless further evaluated.

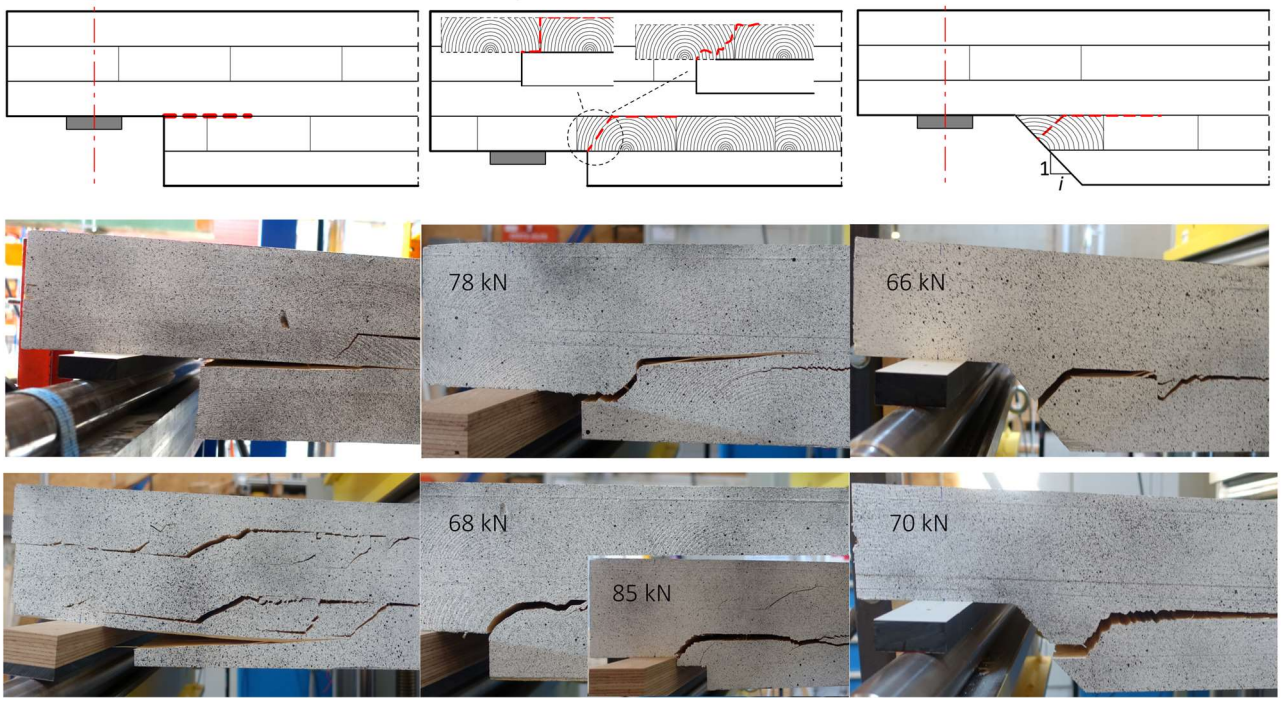

Figure 5 *Left: Failure mode in longitudinal layer and failure due to the rolling shear failure in series 5F at bottom left; Middle: Different failure modes in transversal layer for series 5E; Right: Different failure modes in tapered notch series 5D**

3.3.2 Tests on reinforced notches

3.3.2.1 General

The reinforcement consisted for all reinforced series of self-tapping screws with a diameter d = 8 mm and was placed at a distance of 2.5d from the notch tip in order to increase on one hand the effectiveness of the reinforcement as reported in Augustin (2016), and on the other to avoid a splitting of the member at the end face. The number of screws, all applied in a row, was varied depending on the expected load carrying capacity and ranged from 2 to 4 equally spaced screws.

For series 5A-R2, 5A-R3, 5C-R1, 5C-R2 the number of screws or side from which screws were applied was varied. In order to reduce the influence of material parameters these variations were made on each specimen, e.g. one side of the specimen was tested with two screws and other side with four.

3.3.2.2 Test results

In Table 3 the results of the test series with reinforced notches are listed.

Table 3. Detailed results of tests on reinforced notches

Series		5A-R1	5A-R2	5A-R3[a)]	5C-R1		5C-R2[a)]		7A-R	7C-R
Screw	n_{screw}	4	4		2	4	2	4	3	3
	$F_{, axial}$ [kN]	31.8	23.2	23.2	12.2	24.4	8.5	17.1	24.4	27.5
	d [mm]	8.0								
Screw angle ϕ		45	90		90				90	90
β			0.40		0.40				0.40	0.40
α			0.50		0.60				0.62	0.57
$V_{f, r, mean}$	[kN]	84.0	78.0	79.8	80.2	92.6	80.3	88.5	105	100
V_{crack}	[kN]	60.0	45.0		60.0				60.0	70.0
Num. of tests		6	5	5	4	5	4	5	6	6
CoV	[%]	5.64	1.83	5.77	5.48	4.92	5.94	5.37	5.05	7.10
$V_{f,005}$	[kN]	74.9	75.2	70.7	71.4	83.6	70.8	79.4	94.7	86.6
MIN	[kN]	78.0	76.0	73.5	77.5	87.5	74.6	79.9	99.0	92.0
MAX	[kN]	91.5	80.0	87.5	87.8	100	85.0	94.2	115	112
$V_{f, r, mean}$ / $V_{f, ref}$ [b)]	[%]	79.2	73.6	75.3	75.7	87.4	75.8	83.5	92.9	69.4
$V_{f, r, mean}$ / $V_{f, mean}$ [c)]	[%]	175	162	166	113	131	114	125	140	137

a) Screws applied from the top side of the plate

b) Reference failure load is referred to rolling shear failure of unreinforced "REF" series

c) mean failure load of the unreinforced notch with the same notch parameters

3.3.2.3 Fracture behaviour of the reinforced notches

During the tests on the reinforced specimen a significant increase of the failure load could be observed in comparison to the tests with unreinforced notches. The load at crack initiation was however similar to the unreinforced notches, implying that the reinforcement contributes to load-bearing capacity and crack growth stability only after the initial crack growth. A similar behaviour is reported in Jockwer (2014) and Augustin (2016). The explanation for this behaviour can be found in the singular behaviour of stresses around the notch tip and the small deformation in the vicinity of reinforcement prior to the crack initiation. This assumption was confirmed by the DIC measurements.

It has to be noted that, although the load-bearing capacity significantly increased with the reinforcement, the full load-bearing capacity of the reference specimen without the notch, failing in rolling shear, could not be achieved.

The failure mode of the reinforced notched CLT elements was identified as screw withdrawal failure, accompanied by a subsequent instable crack growth. This implies that for the tested notch and screw parameters the withdrawal strength of the screws is the critical property.

The reinforced CLT notches showed a steady crack growth after crack initiation leading to a stable behaviour of the specimens. The crack length at failure, determined by the DIC software, was around 90 mm. Compared with the steady crack growth length in the unreinforced notches of around 20 mm, this is significant higher.

A detailed analysis and derivation of an analytical model for estimation of the load-bearing capacity of the reinforced notches was not done within the scope of this paper and will be made in the future.

4 Analytical and Numerical models

The following calculations of analytical and numerical models were performed with the material properties given in Table 4. It is noted that these properties, especially the fracture energies, are not calibrated because no fracture energy tests on small specimen were carried out. No distinctions between radial and tangential directions were made regarding stiffness and fracture properties.

Table 4. Used material properties for the analytical and numerical models

Parameter	Value	Description
E_0 ; E_{90}	11000 ; 390	MOE longitudinal; transversal [MPa]
$G_{0,90}$; $G_{90,90}$	690 ; 69.0	Shear modulus, longitudinal; transversal [MPa]
$f_{t,90}$	2.00	Strength in tension, perp to grain [MPa]
$f_{v,0}$, $f_{v,r}$	4.00 ; 2.00	Shear strength, along the grain ; rolling shear [MPa]
$G_{c,I}$; $G_{c,II}$	0.30 ; 1.20	Critical energy release rate, Mode I ; Mode II [mJ/mm^2]
$\nu_{,LR}$; $\nu_{,RT}$	0.56 ; 0.03	Poisson ratios [-]

4.1 Numerical investigations

The unreinforced notch configurations from Table 2 were analysed with the FEM analysis software package "Ansys Mechanical 2020R2". Two different numerical methods were performed using the built in software code for fracture mechanics:

- 2D Plane Stress model based on linear elastic Virtual Crack Closing Technique (VCCT)
- 2D Plane Stress nonlinear contact debonding tool using Cohesive Zone modelling (CZM).

The used numerical model is presented in Figure 6. A mesh convergence study was performed around the notch in order to optimize the mesh size for the computation. The mesh refinement around the notch was made with elements of 0.2 mm in size. In parts of the CLT element not influenced by the stress concentrations at the notch the mesh size is determined depending on height of the intact beam. Only half of the specimen was considered in the analysis using symmetry boundary conditions in order to reduce computation time. The supports were modelled as a non-sliding contact between the steel plate support and CLT element. The steel plate is restrained with

roller support (u_x = Free, u_y = 0, φ_z = Free). The different contacts between the steel plate and timber were utilised to investigate the influence of support restrictions on the result, however no influence on results was found. The considered numerical fracture models require a predefined crack tip and crack path. For notches in the longitudinal layer a crack path parallel to the grain was implied, while for a notch in the transversal layer the crack was assumed to propagate at 45° through the transversal layer until the next interface is reached. Afterwards the crack propagates along the interface (see Figure 5, middle). The assumption of 45° angle is reasonable as no distinctions were made between radial and tangential directions in the material properties.

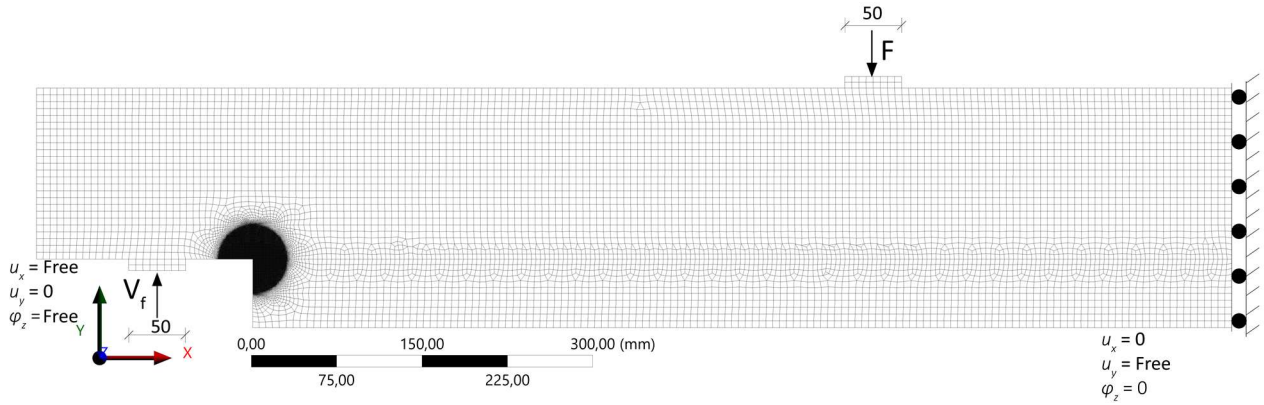

Figure 6 Numerical model used in numerical analysis with coresponding boundary conditions

Both models were investigated using mixed mode conditions with the objective to determine the influence of mode II on fracture. The failure load is computed using failure criteria for mixed mode delamination. Due to limitations of the used software to consider contact debonding a linear elastic failure criterion was used (Eq. (7)).

$$\left(\frac{G_I}{G_{c,I}}\right)+\left(\frac{G_{II}}{G_{c,II}}\right)=1 \tag{7}$$

Although for VCCT several mixed mode fracture criteria are available (e.g. exponential criteria) the linear criteria was applied in both approaches in order to compare two numerical approaches.

The considered models showed, overall, different results: The VCCT model overestimates the failure load of the test specimen by a factor of 1.2 to 1.3. An explanation for this behaviour can be found in the fact, that the fracture process zone is not considered in VCCT. Furthermore, VCCT in general overestimates the results as infinite strength of the material is assumed ($f_{t,\,90} = \infty$). The load-bearing capacity is even more exceeded for large α and small β, where for series 5F the failure is 1.8 times higher. Since the specimen of series 5F and 3A failed in rolling shear, i.e. a different failure mode, such extreme values are of no concern. A better correspondence with the test results can be achieved by increasing the crack length for the length of the process zone. A similar approach was used in Serrano (2019, 2020) from which it can

be seen that without a modification of the crack length the failure loads for some notch configurations are overestimated.

The modelling using the CZM showed, in general, a good correspondence with the test results, illustrating the influence of process zone in timber.

The results from the numerical analysis will be presented in section 5.1.

4.2 Analytical models

The comparison of results from Eq. (6) with previous test campaigns given in Serrano (2019, 2020) give promising implications regarding the applicability of Eq. (6) as a design equation. However, if the fitting parameter Δa is not considered, the failure loads in general are overestimated, and for a certain domain of α and material properties even unphysical results showing higher failure loads or complex solutions, are possible (Figure 10 right). Due to these reasons the fitting parameter can't be omitted from the analysis and it needs to be investigated in detail over relevant parameter domain in order to implement it in the next generation of codes. Experimental and numerical testing on numerous layups and different notch parameters becomes exponentially difficult due to the heterogeneity of CLT, therefore in this paper an analytical solution is presented for the evaluation of the fitting parameter Δa. This approach describes the additional rotation of the cross section at the crack tip, in literature often deduced as *beam root* rotation.

4.2.1 Elastic interface semi-rigid model

The analytical solution is based on the work of Qiao and Wang (2004) and it represents a solution according to the energy balance method of LEFM on two shear deformable bi-layer beams coupled at the interface considering appropriate kinematic conditions, (see Figure 7). Depending on these conditions at the interface three different levels of solutions, each rising in complexity, can be obtained.

The main kinematic conditions at the interface of the two beams can be expressed as

$$\varphi_1 = \varphi_2 \text{ and } u_1 - \varphi_1 \frac{h_1}{2} = u_2 + \varphi_2 \frac{h_2}{2}, \tag{8}$$

where φ_i denotes the rotation of beam 1 above the crack and beam 2 under the crack, u_i stands for the longitudinal displacements along the interface and h_i is equal to the height of the beams.

The mentioned three levels of solution are defined as:

Rigid model: This is the simplest model considering both kinematic conditions of Eq. (8) at the crack tip. This is completely equivalent to the solution of the Structural Element Model in case when k_φ approaches infinity and Δa = 0.

Semi-rigid model: This model releases the boundary condition $\varphi_1 = \varphi_2$ causing the independent rotation of the coupled beams, but considers the displacement continuity condition.

Flexible model: In this approach both kinematic boundary conditions are modified. The solution is improved by taking into account the deformability of the interface by introducing continuously distributed normal and shear springs at the interface boundary. As a consequence, the normal and shear stresses at the interface are proportional to the spring stiffnesses.

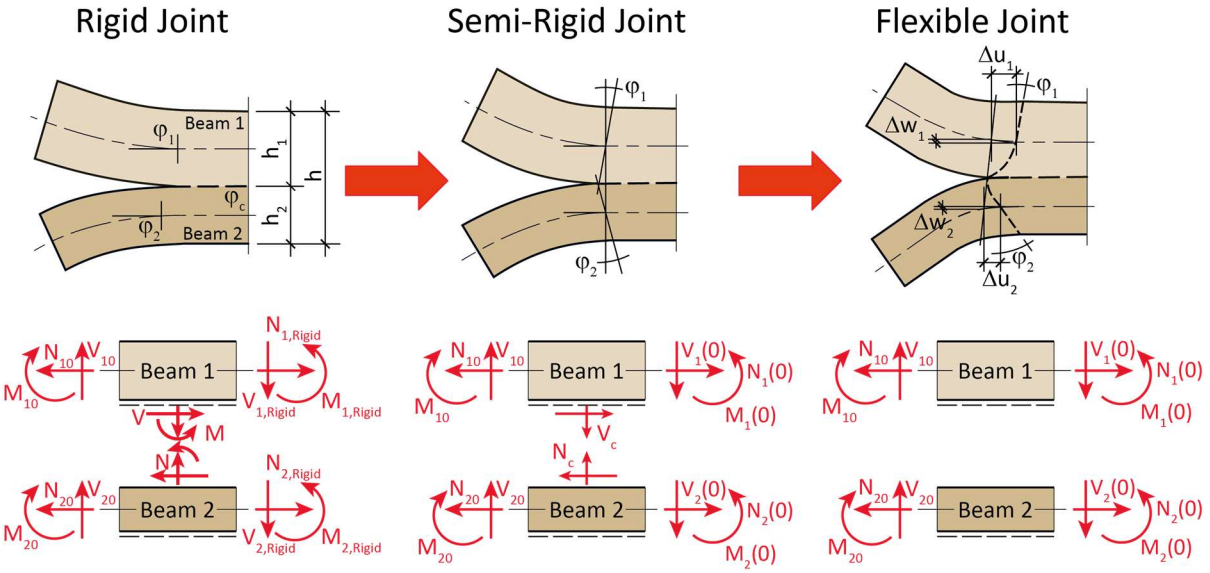

Figure 7 Depiction of crack tip element of joint models in a bi-layer beam system

In the following the beam root rotation in CLT is investigated with the help of the semi-rigid model. This can be interpreted as a good trade-off between complexity and accuracy of the model. Only the main solutions regarding this model will be given in order to keep the paper in a reasonable scale. For a detailed derivation of the mentioned models refer to Qiao and Wang (2004).

By differentiating Eq. (8), taking into account the constitutive equations of the Timoshenko beam theory and considering the equilibrium conditions $\Sigma M = 0$, $\Sigma V = 0$, $\Sigma N = 0$ at the crack tip element (CTE) in Figure 7., the governing equation of the semi-rigid joint model is obtained as

$$\left(\frac{1}{(\kappa GA)_1}+\frac{1}{(\kappa GA)_2}\right)\left(\eta+\frac{\xi h_1}{2}\right)\frac{d^2N_1(x)}{dx^2}-\left(\left(\frac{1}{(EI)_1}+\frac{1}{(EI)_2}\right)\eta+\frac{(h_1+h_2)}{2(EI)_2}\xi\right)N_1(x)=-q(x)$$

$$q(x)=\left(\left(\frac{1}{(EI)_1}+\frac{1}{(EI)_2}\right)\frac{h_2}{2(EI)_2}+\frac{\xi}{(EI)_2}\right)M_{10}+\left(\frac{1}{(EI)_1}+\frac{1}{(EI)_2}\right)\frac{N_{10}}{(EA)_2}, \tag{9}$$

where

$$\xi=\frac{1}{2}\left(\frac{h_1}{(EI)_1}-\frac{h_2}{(EI)_2}\right),\ \eta=\frac{1}{(EA)_1}+\frac{1}{(EA)_2}+\frac{(h_1+h_2)h_2}{4(EI)_2},\ M_{10}=V_f\beta h,\ N_{10}=0$$

The solution of Eq. (9) considering a semi-infinite long beam is

$$N_1(x) = ce^{-kx} + N_{1,RIGID} \text{ , where} \tag{10}$$

$$c = \frac{(2M + h_1 N)\xi}{h_1\xi + 2\eta}, \qquad k = \sqrt{\frac{(\kappa GA)_1 (\kappa GA)_2 \left\{2\left((EI)_1 + (EI)_2\right)\eta + (EI)_1 (h_1 + h_2)\xi\right\}}{(EI)_1 (EI)_2 \left((\kappa GA)_1 + (\kappa GA)_2\right)(2\eta + h_1\xi)}}$$

M, N form a group of self-equilibrating forces at the CTE describing the deformation of the crack tip obtained by imposing equilibrium conditions on CTE in Figure 7, middle.

At the crack tip the beam root rotation can be computed as

$$\Delta\varphi_1 = \varphi_1(0) - \varphi_{1,\,RIGID}(0) = \int_0^L \frac{M_1}{(EI)_1}\,dx - \int_0^L \frac{M_{1,\,RIGID}}{(EI)_1}\,dx\,. \tag{11}$$

According to the principle of superposition in LEFM the ERR of the semi-rigid joint can be obtained from the summation of the compliances of the rigid model, already presented in Eq. (6) (for case $\Delta a = 0$), and the additional contribution of the beam root rotation (Figure 8). The ERR due to the beam root rotation is thus defined as

$$G_{c,\,crack\,rotation} = \frac{V_f^{\,2}}{2B}\frac{dC_{c,\,crack\,rotation}}{da} = \frac{V_f^{\,2}}{4B}(\Delta\varphi a + \Delta w) \tag{12}$$

The closed form of the failure load at the support including the contribution of the rigid model and beam root rotation, leads, after simplification of Eq. (11) and Eq. (12) to

$$V_f = \sqrt{\frac{2BG_c}{\frac{1}{4}\left(\left(\frac{1-\psi}{(EI)_1}(\beta h)^2 + \frac{1-\rho}{(\kappa GA)_1}\right) + \left(\frac{\left(2(1-\psi) - h_1 A_N\right)}{h_1\xi + 2\eta}\right)\cdot\left(\frac{2\eta a}{(EI)_1 k} + \frac{\eta}{(EI)_1 k^2} - \frac{1}{(\kappa GA)_1}\left(\eta + \frac{h_1\xi}{2}\right)\right)\right)}} \tag{13}$$

where $\psi = \frac{(EI)_1}{(EI)_3}$, $\rho = \frac{(\kappa GA)_1}{(\kappa GA)_3}$ and $A_N = \frac{\left((EI)_1 + (EI)_2\right)h_2 + 2(EI)_1(EI)_2\xi}{2(EI)_2\left((EI)_1 + (EI)_2\right)\eta + (EI)_1(EI)_2(h_1 + h_2)\xi}$

Remark: The closed form solution can be used in future for a parametric analysis and a verification of the fitting parameter developed in Serrano (2019).

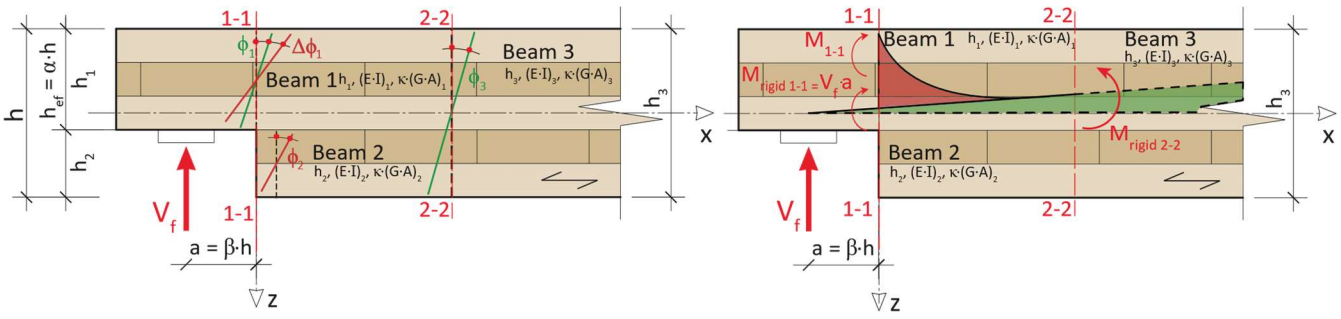

Figure 8 Ilustration of the beam root rotation and the subsequent local concentrations of internal forces

4.2.2 *Beam on elastic foundation*

An alternative approach to the Structural Element Model can be deduced based on a Timoshenko beam on elastic foundation (BEF) taking into account an adaption for the case of an unreinforced notched CLT plate (Figure 9).

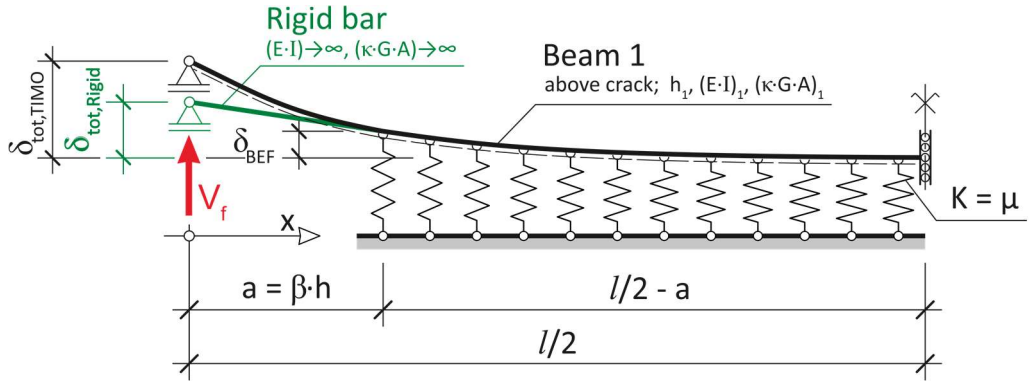

Figure 9 Timoshenko beam on elastic foundation

The model consists of two structural parts:

Beam 1 in the BEF is denoted as part of the CLT beam above the crack. The springs with the spring constant K represent the elastic delamination of the interface at the crack tip and along the delamination plane. The fracture layer is assumed to be coupled with a stiff foundation. The part of the beam under the crack is ignored.

Second structural part is a rigid bar representing the cantilever part of the Beam 1. With introduction of rigid bar the deformation of the cantilever beam is defined with deformation of the BEF at the crack tip, while the deformation of the cantilever itself is ignored. This assumption is supported by the poor matching with test result when the Timoshenko cantilever beam is considered making the failure loads over conservative. However, it is noted that the results matched well for $\alpha < 0.3$.

To consider deformation of the beam under the crack and in front of the crack the modification of spring stiffness μ is introduced. Furthermore in Eq. (18) the exponent m is introduced as function of notch length β taking into account the assumption of rigid bar. For domain of β where m is not explicitly defined the linear interpolation is allowed.

$$\mu = \frac{K}{(1-\alpha)^m}, \text{ where } m = \begin{cases} 1 \ for \ \beta \le 0.3 \\ 3 \ for \ \beta \ge 0.4 \end{cases}. \tag{18}$$

K is the foundation modulus [N/mm^3] and it is derived from the analysis presented in Augustin (2016) leading to $K \approx 2$ [N/mm^3].

The interface stress at the notch tip according to the BEF can be calculated as

$$\sigma_y(x) = K w_y(x). \tag{14}$$

The general solution of Timoshenko beam on elastic foundation as well as the differential equation are left out in order to reduce the scope of this paper. A detailed derivation can be found in the work of Jorissen (1998).

Solving the differential equation of BEF and introducing the boundary conditions from Figure 9. ($M_{1,\,x=\beta h} = V_f \beta h$, $P_{1,\,x=\beta h} = V_f$) leads to a solution for the deformation at the end point of BEF, i.e. the crack tip, expressed as

$$w_y(x) = -\frac{2V_f}{\mu B}\left(\gamma + \lambda^2 \beta h\right), \tag{15}$$

where

$$\gamma = \sqrt{\lambda^2 + \frac{\mu B}{4(\kappa GA)_1}} \quad \text{and} \quad \lambda = \sqrt[4]{\frac{\mu B}{4(EI)_1}}.$$

Analogue to the deformation an equation for the rotation at the crack tip can be obtained as

$$\varphi = \varphi_{(0)} = -V_f \left(\frac{1}{2EI\lambda^2} + \frac{\beta h}{\gamma}\left(\frac{\lambda^2}{(\kappa GA)_1} + \frac{1}{(EI)_1} \right) \right). \tag{16}$$

The total deformation at the loading point from Timoshenko BEF is then

$$\delta_{total} = w_{y(0)} + \beta h \varphi_{(0)}. \tag{17}$$

Combining Eq. (15 to 17), deriving the expression with respect to the crack length βh and solving the equation with help of Eq. (2) the failure load can be obtained as

$$V_f = \sqrt{\frac{2BG_c}{2\frac{\beta h}{\gamma}\left(\frac{\lambda^2}{(\kappa GA)_1} + \frac{1}{(EI)_1} \right) + \frac{1}{(EI)_1 \lambda^2}}}. \tag{19}$$

5 Model comparison with experimental results

5.1 Comparison of analytical and numerical results of unreinforced notches

The following comparison of analytical and numerical results with test results on unreinforced CLT notches is conducted on the basis of mean values.

The distribution of the failure load at the support for different analytical models is illustrated in Figure 10, left. The distribution is shown for the 30-30-30-30-30 layup.

The comparison of the experimental test with the mentioned analytical and numerical methods is depicted in Figure 11.

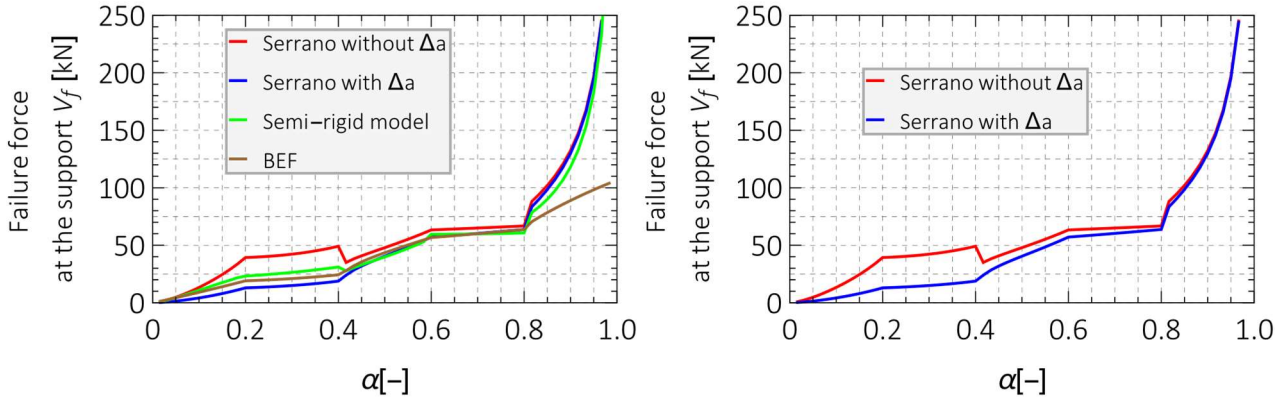

Figure 10 Left: Distribution of failure forces at the support depending on the parameter α for developed analytical models; Right: Comparison of the Structural Element Model with and without fitting parameter

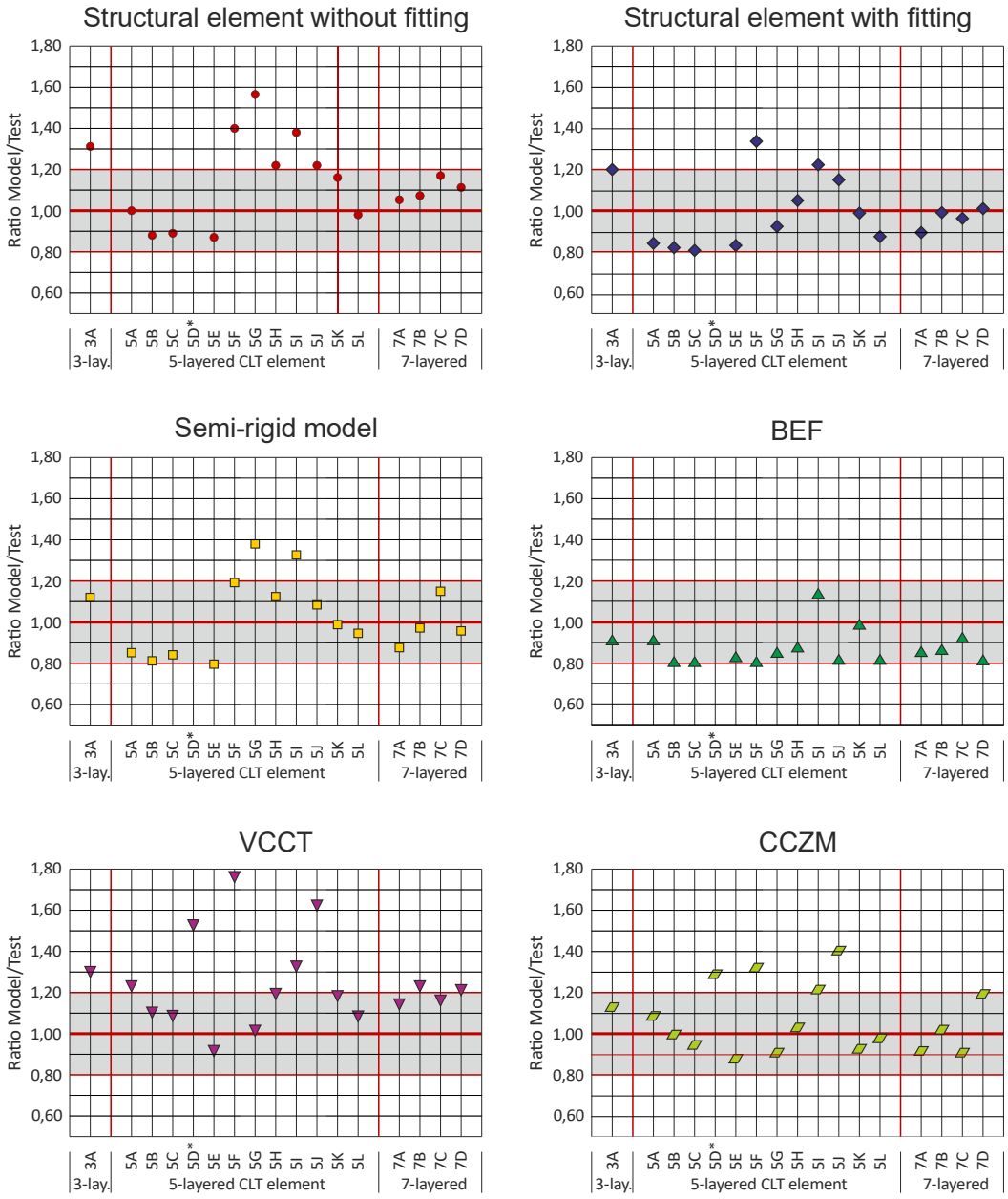

Figure 11 Comparison of results from the developed models with the conducted experimental tests. Ratio V_{f_Model} / V_{f_Test} is shown, if ratio > 1 the failure load is overpredicted by the model results, i.e. on the unsafe side

Before coming to the comparison of results, it should be emphasised that no calibration of material properties was made. As a general statement it could be determined from the comparison that the developed models match good with the experimental tests. The results are for most of the series positioned on the conservative side, excluding series 5I and 5H. It is evident that the mentioned series were delivered from the same producer. Thus it can be suspected, that these series consisted of a different material with weaker properties, i.e. smaller fracture energy. All the specimens of series 5F, 3A, failed in rolling shear, consequently making a direct comparison of the failure loads at the notch unclear. All other series failed by delamination at the notch making the comparison valid.

The Structural Element Model without fitting (rigid model) presented unsafe results for 7-layer members and series 5G, while this model with consideration of the fitting parameter provided better results proving applicability of developed Δa also for this domain of tested parameters in addition to the tests in Serrano (2020, 2019).

In comparison the semi rigid model and Structural Element Model with fitting factor provided in general the same behaviour in the domain of considered layups and notch parameters, excluding the series 5G. This can be explained by the high sensitivity of the semi rigid model on ratio of shear stiffnesses $(\kappa GA)_1/(\kappa GA)_2$.

The BEF model provided more conservative results of failure loads due to the crude assumption of a rigid bar and that of the stiff foundation. It seems that the considered modification of the foundation stiffness isn't enough to overcome the used assumptions. Better results can be obtained, if one considers Vlaslov beam on elastic foundation due to the included rotational springs (Yoshida 2018). It is further noted that, the solution of BEF seems to be applicable only if $\beta < 0.6$ due to the made assumptions. For solutions out of this domain, results on the conservative side are obtained when comparing to other mentioned models.

The numerical model according to VCCT overestimate the fracture loads in almost all series by a significant factor. Considering the additional length of process zone yields to better result. The additional crack length of 15 mm is chosen for series 5A and failure load was overestimated for factor 1.05 in comparison to 1.3 when no modification was considered. The additional crack length is evaluated based on nonlinear fracture mechanics. It should be noted that on results of VCCT the assumption of linear mixed mode fracture criteria plays a role.

The CZM model showed good matching with test results in domain of notches not influenced by rolling shear failure.

The assumption of $G_c = G_{c,I}$ showed a good approximation as the mixed mode failures computed in numerical analyses didn´t show significant influence of mode II on failure loads. The mode mixity in CLT notches can also be calculated in an analytical way with the help of semi-rigid model.

6 Conclusion and recommendations for design and further work

The following conclusion can be drawn from the present work:

- The Structural Element Model in general gives good matching with test results over different layups, proving the robustness of the fitting parameter Δa.
- A fitting parameter can be verified through the parametric analysis utilizing model developed in this work.
- The VCCT approach overestimates the load-bearing capacity. An additional crack length should be considered for this model.
- The current models given in ETA-06/0138 and Wallner-Novak are not appropriate due to wrong theoretical assumptions. A fitting of the factor k_n would work only on a limited number of layups.
- The current provisions in ETA-06/0138 regarding limit values of geometrical notch parameters seem inadequate for layered structure of CLT. In that direction the following recommendations for limiting values could be:
  - for 3 layered plates: up to 2/3 of first (bottom) layer may be notched; $\beta \leq 0.6$; in case of a deeper notch reinforcement shall be used.
  - for 5 layered plates: $\alpha \geq 0.5$; $\beta \leq 0.6$; if the first (bottom) layer is transversal layer reinforcement shall be used.
  - for 7 layered plates: $\alpha \geq 0.5$; $\beta \leq 0.6$, otherwise apply a reinforcement.

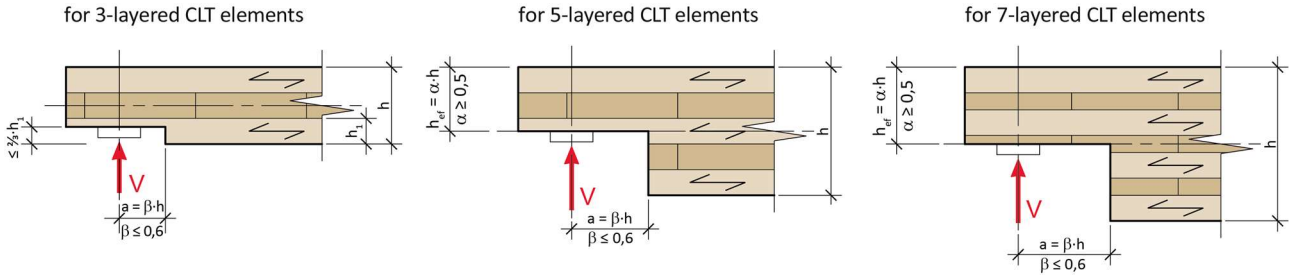

Figure 12 Proposal for limit values of geometric parameters of different lay-ups of CLT elements Remark: The geometric restrictions are valid for main structural direction and secondary direction of the plate (first layer transversal)

- More tests on tapered notches with $i > 1.0$ is needed. Only with large database of the experimental tests on tapered notches the calibration of load-bearing capacity can be made. Similar expression as mentioned in section 3.3.1.1 can be utilized as a basis for the calibration.

Further research should gravitate towards the following topics in CLT notches:

- Calibration of fracture properties in order to further verify the models
- Parametric analysis of a fitting factor Δa with help of a semi-rigid model
- Development of analytical and numerical approaches for the determination of the load-bearing capacity of reinforced notches and force in the reinforcement.

- Investigation of the Duration-of-Load (DOL) behaviour as well as the influence of variation of the moisture content on the load-bearing capacity of notches in natural and varying climates.

7 Acknowledgment

This research work was prepared within the project "Notches in CLT and CLT ribbed panels" which is funded in the program line FFG Collective Research by the Austrian Research Promotion Agency FFG. This support is gratefully acknowledged

8 References

Augustin M., et al. (2016): A Contribution to the Design of Ribbed Plates, World Conference on Timber Engineering, Vienna, Austria

ETA-06/0138 (2017): European Technical Assessment, 20.2.2017

Eurocode 5 (2004): Design of timber structures - Part 1-1: General and rules for buildings. CEN. (EN 1995-1-1).

Friberg, A. (2017): Bärförmåga för KL-trä med urtag–Provning och beräkningsmetoder (in Swedish). (Load-bearing capacity of CLT with notches –Testing and calculation methods). Bachelor thesis, Report THID-5526, Division of Structural Mechanics, Lund University, Sweden

Griffith, A. A. (1921): The phenomena of rupture and flow in solids. Philosophical Transactions of the Royal Society of London, A. 221 (582-593): 163-198

Gustafsson, P. J. (1988): A study of strength of notched beams. In: Proceedings CIB-W18 Meeting 21, Paper CIB-W18/21-10-1, Parksville, Canada.

Jensen, L.J., Gustafsson P.J. (2004): Shear strength of beam splice joints with glued-in rods, J Wood Sci (2004) 50:123–129, Japan, DOI: 10.1007/s10086-003-0538-6

Jockwer, R. (2014): Structural Behaviour of Glued Laminated Timber Beams with Unreinforced and Reinforced Notches, Dissertation, ETH Zurich

Jorissen, A.J.M. (1998): Double shear timber connections with dowel type fasteners, Delft University Press, Delft, Netherlands

Qiao, P., Wang J. (2005): Novel joint deformation models and their application to delamination fracture analysis, Composites Science and Technology 65 (2005) 1826–1839

Serrano, E., Danielsson, H. (2020): Fracture Mechanics Based Design of CLT plates– Notches at Supports and Half and-Half Joints. In: International Network on Timber Engineering Research – Proceedings Meeting 53, Paper INTER/53-12-2, Online.

Serrano, E., Gustafsson, P. J. and Danielsson, H. (2019): Prediction of load-bearing capacity of notched cross laminated timber plates. In: International Network on Timber Engineering Research – Proceedings Meeting 52, Paper INTER/52-12-2, Tacoma, USA.

Wallner-Novak, M., Koppelhuber, J. & Pock, K. (2013): Brettsperrholz Bemessung – Grundlagen für Statik und Konstruktion nach Eurocode (in German). ProHolz Austria, Vienna, Austria.

Yoshida, K., Takahira, A. (2018): Beam on elastic foundation analysis of sandwich SCB specimen for debond fracture characterization, Composite Structures Volume 195, 1 July 2018, Pages 83-92, DOI: https://doi.org/10.1016/j.compstruct.2018.04.032